

Design for the Mechanical Properties of Polypropylene Discontinuous Fiber-Reinforced Cementitious Composites Manufactured by Extrusion Molding

H.Takashima & K.Miyagai

Technical Research Laboratory, Kurabo Industries Ltd., Osaka, Japan

T.Hashida

Fracture Research Institute, Graduate School of Engineering, Tohoku University, Sendai, Japan

V.C.Li

Advanced Civil Engineering Material Research Laboratory, Department of Civil and Environmental Engineering, The University of Michigan, Ann Arbor, MI, USA

ABSTRACT: Polypropylene discontinuous fiber reinforced cementitious composites were prepared by extrusion molding and tested in uniaxial tension to determine the mechanical properties such as ultimate composite strength and strain, and the critical volume fraction for multiple cracking. It was shown that the experimentally determined critical fiber volume fraction reasonably agreed with theoretical value predicted by a micromechanics model conducted in this study. The extruded fiber composites are yielded the ultimate composite strength of 8.9MPa and the composite strain of 0.55% at the fiber volume fraction of 7.4%. Our experimental results suggest that there is the apparent bound for suitable fiber volume fraction.

1 INTRODUCTION

Extrusion molding has a potential of producing fiber reinforced cementitious composites with higher performance compared with the conventional traditional molding. There are two major advantages of extrusion molding in manufacturing fiber composites: lower porosity of extruded composites due to mechanical compaction, and aligned orientation of fibers. The lower porosity may increase the composite strength and matrix brittleness. In addition, the aligned fiber orientation may enhance the mechanical properties of fiber composites in the extrusion direction. One of the most effective ways for improving the brittleness of cementitious composites is the use of multiple cracking phenomenon induced by fiber reinforcement. The multiple cracking phenomenon produces pseudo strain-hardening behavior characterized by a sustained and increasing load capacity after first matrix crack (Aveston & Kelly 1973).

A general micromechanics model has been developed for random short fiber composites based on fracture mechanics approach (Li et al. 1991, Li 1992a, Li & Leung 1992b, Stang et al. 1995, Kabele & Horii 1996). The micromechanics model has been validated by experimental investigations (Li & Hashida 1993, Kanda et al. 2000).

In contrast, the design methodology for discontinuous fiber cementitious composites by extrusion molding has not been established yet. The composite parameters such as matrix and fiber parameters are being selected by a try and error approach. There are few research investigated a theoretical model for extruded discontinuous fiber reinforced cementitious

composite (Stang & Pedersen 1996, Mu & Li 1998, Li et al. 1999). Mu & Li (1998) and Li et al. (1999) have reported their theoretical models for predicting the bend over point stress and the condition for multiple cracking for aligned short fiber reinforced composites based on an energy approach and inclusion method. They showed that the bend over point stress predicted by their model was close to the experimental value. However, the theoretical model for the condition of multiple cracking has not been validated experimentally yet.

Shah & Shao (1994), Shao et al. (1995) and Akkaya et al. (2000) have reported that discontinuous fiber-reinforced cementitious composites manufactured by extrusion showed pseudo strain-hardening behavior. However, no attempt has been made to develop a theoretical model for the design of extruded fiber reinforced composites.

In this paper, we take advantage of the micromechanics model based on a fracture mechanics approach (Li et al. 1991, Li 1992a, Li & Leung 1992b) to design the mechanical properties of discontinuous fiber reinforced composite by extrusion molding, especially to predict the necessary condition for pseudo strain-hardening behavior. We prepared extruded fiber composite using fibers. Direct tension tests were carried out to determine the mechanical properties such as ultimate tensile stress and strain, and the critical fiber volume fraction of the extruded composites. The experimental data were compared with theoretical prediction based on the micromechanics model. The mechanical properties of the extruded composites were also compared with those of cast fiber composites in terms of interfacial friction bond strength.

2 THEORY

In this paper, we adopt a simple model of fiber matrix interface debonding based on a purely interfacial friction bond strength ignoring elastic bond. The following assumptions are made to construct the micromechanics model. Firstly, fibers never break. Fibers are debonded and pulled out completely from the matrix. Secondly, the interfacial friction bond strength along the fiber-matrix interface is constant during the debonding and pulled out process.

Li (1992a) has analyzed the relationship between the fiber bridging load and displacement during fiber frictional debonding and pullout. We adopt this relationship to aligned fiber composites. The prepeak and postpeak part of the bridging stress-displacement curve $\sigma_B\text{-}\delta$ can then be obtained in a normalized form (See Appendix):

$$\tilde{\sigma}_B(\tilde{\delta}) = 2 \left[2 \left(\frac{\tilde{\delta}}{\tilde{\delta}^*} \right)^2 - \frac{\tilde{\delta}}{\tilde{\delta}^*} \right] \text{ for } \tilde{\delta} \leq \tilde{\delta}^* \quad (1)$$

$$\tilde{\sigma}_B(\tilde{\delta}) = 2(1 - \tilde{\delta}) \text{ for } 1 > \tilde{\delta} > \tilde{\delta}^* \quad (2)$$

where $\tilde{\sigma}_B \equiv \sigma_B / \sigma_0$, $\sigma_0 \equiv V_f \tau (L_f / d_f) / 2$, and $\tilde{\delta} \equiv \delta / (L_f / 2)$. $\tilde{\delta}^* \equiv [2\tau / (1+\eta) E_f] (L_f / d_f)$ corresponds to the maximum attainable value of δ_0 normalized by $L_f / 2$ for the fiber with the longest embedment length of $L_f / 2$. d_f = fiber diameter, L_f = fiber length, τ = an interfacial friction bond strength. The elastic modulus of matrix and fiber are E_m , E_f , respectively and the volume fraction matrix and fiber are V_m , V_f , respectively. $\delta_0 \equiv (4l^2\tau) / [(1+\eta) E_f d_f]$ correspond to the displacement at which frictional debonding is completed for a fiber with embedment length l and $\eta \equiv (V_f E_f / V_m E_m)$.

Marshall & Cox (1988) have shown that based on J-integral method the crack tip toughness J_{tip} during steady state cracking can be expressed by:

$$J_{tip} = \sigma_a \delta_a - \int_0^{\delta_a} \sigma_B(\delta) d\delta \quad (3)$$

where σ_a = steady state cracking stress and δ_a = the displacement corresponding to σ_a .

Li (1993) reviewed the necessary conditions of fiber fraction for pseudo strain-hardening behavior. For pseudo strain-hardening with multiple cracking,

$$\sigma_a \leq \sigma_{pc} \quad (4)$$

$$J_{tip} \leq \sigma_{pc} \delta' - \int_0^{\delta'} P(\delta) d\delta \quad (5)$$

where σ_{pc} = the maximum value of the bridging stress-displacement curve.

Using eqs. (1) and (2) in eq. (5), the critical fiber volume fraction $V_{f,crit}$ for multiple cracking is given by:

$$V_f \geq V_{f,crit} = \frac{6d_f^2 E_f (1+\eta)}{\tau^2 L_f^3} J_{tip} \quad (6)$$

3 EXPERIMENTAL PROCEDURE

3.1 Materials

The mix proportion of the matrix is shown in Table 1. All of the mix proportions are by weight of the ingredients. Discontinuous polypropylene fibers with various volume fractions (0-8.4%) were employed in this study. The fiber dimensions and properties are shown in Table 2.

3.2 Specimen preparation

In this paper, the mechanical properties of fiber reinforced composites manufactured by extrusion were compared with cast fiber composites. These composites were made of the same proportion of raw materials. The preparation for these composites is presented below.

Table 1. Matrix Mix Proportion (by weight).

Ordinary Portland Cement	Silica Powder	Mineral Pulp	Methyl Cellulose	Water
1.00	0.64	0.05	0.05	0.77

Table 2. Dimensions and properties of fiber used.

Fiber Type	Length L_f (mm)	Diameter d_f (mm)	Young's Modulus E_f (GPa)	Tensile Strength σ_f (MPa)
Poly Propylene	6	0.018	3.7	295

Firstly, the raw materials were mixed for three minutes without water by an Erich mixer. Water was added into the mixture and mixed for two minutes. The mixture was used to prepare the fiber composites by casting.

Next, the mixture is kneaded for three minutes by a kneader with two blades. The kneaded mixture was used to prepare the extruded fiber composites. The extrusion molding was conducted using a ram ex-

truder. The extruded samples had the cross section of 80mm × 15mm. The extruded specimens were cut into a length of 250mm perpendicular to the extrusion direction.

Cast fiber composites were prepared using a polyethylene mold. All the specimens were machined into a rectangular coupon of size 230mm × 40mm × 15mm.

The specimens of the extruded and cast composites are steam-cured for four hours at 70°C.

3.3 Testing procedure

The tensile behavior of composites was determined by conducting in uniaxial tension tests. The coupon specimens were tested under displacement control in a 50kN material testing system. The displacement rate used was 0.2mm/min. Aluminum plates were glued by epoxy resin onto the end of the tension specimens. A linear variable differential transducer was used to measure the displacement between two points on the specimen at a gage length of 50mm. Three specimens were tested for the same fiber volume fraction and the results were averaged. The experimental data presented in the following sections are averaged data.

3.4 Fiber orientation and Fiber volume fraction

The cross section perpendicular to the extrusion direction was observed by scanning electron microscopy (SEM) using both extruded and cast composites in order to examine the fiber orientation and fiber volume fraction. As shown in Figure 1, it is possible to determine the distribution of fiber orientation based on the fiber shape of cross section perpendicular to the extrusion direction, because the polypropylene fibers has an exact circular cross section. The orientation of each fibers axis with respect to the plane perpendicular to the extrusion direction, θ is estimated by approximating the fiber cross sec-

tion as an elliptical shape, and given by the following equation:

$$\theta = \sin^{-1}\left(\frac{b}{a}\right) \quad (7)$$

where a and b are the major and minor axis, respectively. Computably aligned fibers with respect to the extrusion direction correspond to 90 degree.

The fiber volume fraction was computed from fiber cross sectional area. The fiber volume fraction determined using cross sections is denoted by $V_{f,real}$.

4 RESULTS AND DISCUSSION

4.1 Fiber orientation

Fiber orientation is one of most important factor for mechanical properties of fiber-reinforced composites. Figure 2 (a) and (b) show an example of SEM scattering observations for the extruded and cast composite, respectively. The polypropylene fibers are observed as dark spots in the photographs.

The distribution of fiber orientation was determined from the SEM observations of cross sections perpendicular to the extrusion direction as described in Experimental Procedure. The distribution of fiber orientation obtained for the extruded and cast composite is shown in Figure 3. The volume fraction $V_{f,real}$ of the extruded composite is 3.1% and 3.3% for the cast composite. It is noted in the extruded composites that approximately 80% of the fibers are aligned with respect to the extrusion direction. The percentage of aligned fibers was almost the same in other extruded composites having fiber volume fraction up to 8.4%. In the extruded composites a broad distribution is seen in the range of 9-63 degree.

The aligned fibers in the extruded composites are expected to have greater influence on the mechanical properties relative to the inclined fibers. In this study, the effective fiber volume fraction $V_{f,eff}$ was calculated by multiplying $V_{f,real}$ by the aligned fiber percentage (approximately 80%) for each extruded composites and used to evaluate the composite mechanical properties based on the micromechanics model.

4.2 Interfacial friction bond strength

In this section, frictional bond strength at the polypropylene fiber / matrix interface was determined from uniaxial tension tests, and the mechanical properties of the extruded and cast composites are compared in terms of the interfacial friction bond strength.

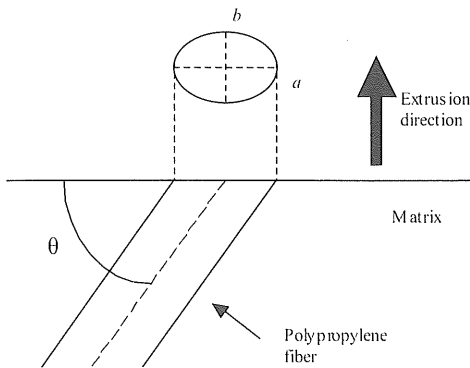
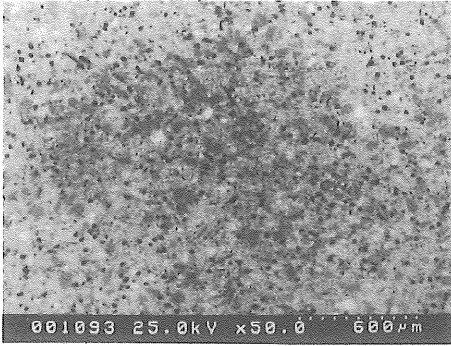


Figure 1. Fiber orientation.

(a) Extruded composite



(b) Cast composite

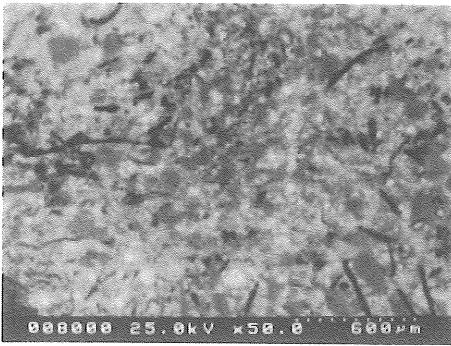


Figure 2. Comparison of microstructures of extruded (a) and cast (b) composites.

Figure 4 shows tensile stress versus strain curves of polypropylene fiber reinforced composites of $V_{f,real} = 1$ and 4.5%, and the matrix prepared by the extrusion molding. The fracture behavior of the matrix and the composite of $V_{f,real} = 1\%$ is characterized by the formation of a single crack, even though the 1% fiber composite shows a gradual stress decrease due to the fiber bridging action. On the other hand, the fiber

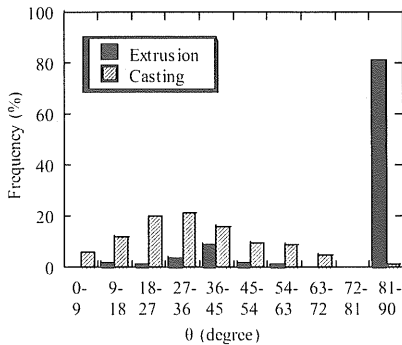


Figure 3. Distributions of fiber orientation of extruded and cast composites.

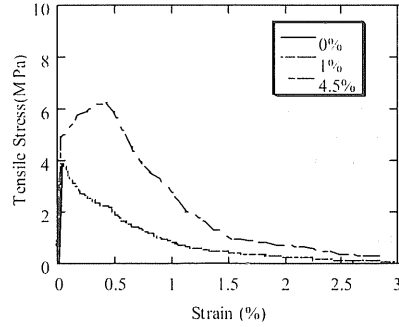


Figure 4. Tensile stress-strain curves of the extruded composites.

composite of $V_{f,real} = 4.5\%$ indicates pseudo strain-hardening behavior due to matrix multiple cracking. The first cracking strength of $V_{f,real} = 4.5\%$ is about 25% higher than that of the matrix only. In particular, the composite strain at peak stress significantly increases up to 1140% compared with the matrix.

In principle, the interfacial friction bond strength is to be determined by conducting a single fiber pull out test (Li & Chan 1994, Kanda and Li 1998). In this study, an estimate of the interfacial friction bond strength τ was obtained from the uniaxial tension tests indirectly.

As detailed in Appendix, the fracture energy due to fiber pullout in aligned fiber composites is expressed by:

$$G_b = \frac{1}{6} \tau V_f d_f \left(\frac{L_f}{d_f} \right)^2 \quad (8)$$

If the fracture energy G_b is determined for aligned fiber composite, the interfacial friction bond strength can then be estimated from the fiber volume fraction and dimensions using eq. (8). G_b may be obtained experimentally based on uniaxial tension tests using the following equation.

$$G_b = \frac{A}{wt} \quad (9)$$

where w = width of the specimen and t = thickness of the specimen. As shown in Figure 5, the area un-

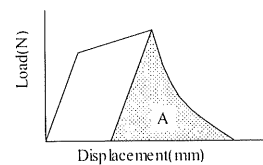


Figure 5. Load-Displacement curve.

der load displacement curve after the peak load is used to determine the area A .

Using eqs. (8) and (9), τ was determined for extruded fiber reinforced composites. For random short fiber reinforced composites, Li (1992a) demonstrated the fracture energy due to fiber pullout:

$$G_b = \frac{1}{12} g \tau V_f d_f \left(\frac{L_f}{d_f} \right)^2 \quad (10)$$

where g = snubbing factor. τ was computed for the cast composites using eq. (10). The value of g was set to be 1.6 in this paper.

Figure 6 shows the dependence of the interfacial friction bond strength τ normalized by initial bond strength by τ_i on the effective fiber volume fraction $V_{f,eff}$. Initial bond strength was determined for the composites of $V_{f,eff} < 1.2\%$. Initial bond strength of the extruded and cast composite was 0.24MPa and 0.30MPa, respectively. In the extruded composites, τ is approximately constant within the range of the fiber volume fractions used in this study. For the cast composites, however, τ decreases rapidly with the increasing fiber volume fraction.

Milewski (1974) and Evans & Gibson (1986) expressed the maximum packing volume fraction $V_{f,max}$ for rod-like reinforcement:

$$V_{f,max} = \frac{5.3}{L_f/d_f} \quad (11)$$

The maximum packing volume fraction is defined on the point at which the randomly oriented fibers have no longer any rotational freedom due to the restrictions of neighboring fibers.

It is expected that the fiber volume fraction greater than $V_{f,max}$, the distributed fibers start to touch each other, causing a reduction in interfacial friction bond strength. The packing volume fraction appears to provide a measure of appropriate volume fraction for producing uniform fiber composites. According to

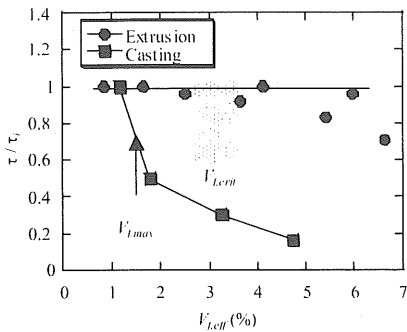


Figure 6. Dependence of τ / τ_i on $V_{f,eff}$.

eq. (11), the value of $V_{f,max}$ becomes 1.6% for the L_f/d_f of 333 used in this study. As shown in Figure 6, τ of the cast composite decreased when $V_{f,eff}$ exceeded $V_{f,max}$.

The comparison may suggest that the extrusion molding allows us to incorporate larger volume of fiber composites compared to the conventional casting.

4.3 Critical fiber volume fraction

Figure 7 shows the number of multiple cracks occurred on the specimens and ultimate tensile strain as a function of $V_{f,eff}$ for the extruded composites. For the composite of $V_{f,eff} < 2.5\%$, only a single crack was observed and multiple cracking phenomenon took place for $V_{f,eff} > 3.6\%$. The critical fiber volume fraction for multiple cracking $V_{f,crit}$ is judged to be in the range of 2.5-3.6%, as indicated in Figure 7.

Theoretically the critical fiber volume fraction for multiple cracking can be obtained from eq. (6). The fiber parameters are shown in Table 2. The interfacial friction bond strength is 0.24MPa. The crack tip toughness J_{tip} in eq. (6) may be approximated as:

$$J_{tip} \approx \frac{K_m^2}{E_m} \quad (12)$$

where K_m = matrix fracture toughness (1.07MPa $m^{1/2}$) and E_m = Young's modulus (21.4GPa).

Eq. (6) yields the value of 3.1% for the critical fiber volume fraction for multiple cracking. It is shown that the critical fiber volume fraction predicted by the micromechanics model reasonably agrees with the experimental results.

4.4 Tensile fracture properties

Figure 8 shows the ultimate tensile stress for the extruded and cast composites as a function of $V_{f,eff}$. The ultimate tensile stress of cast composite showed a relatively constant value regardless of the fiber addi-

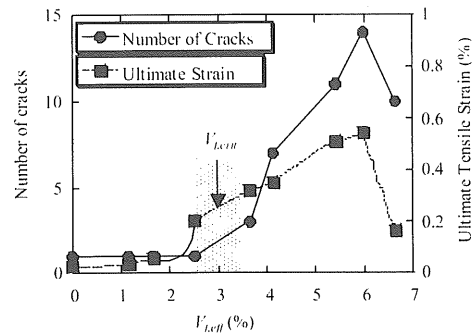


Figure 7. Dependence of number of cracks and ultimate tensile strain on $V_{f,eff}$.

ton and gradually decreased for the fiber volume fraction $> V_{f,max}$, reflecting the reduction in the interfacial friction bond strength. The extruded matrix specimen gave the higher tensile strength than that of the cast matrix, due to the larger density for the extruded matrix (1400 kg/m^3) than 1200 kg/m^3 for the cast matrix. In the extruded composites, the ultimate tensile stress steadily increased with the increasing fiber volume fraction and reaches 8.9MPa at $V_{f,eff} = 6\%$ ($V_{f,real} = 7.4\%$). This ultimate tensile stress 8.9MPa is one of the highest value obtained for extruded discontinuous fiber reinforced cementitious composites.

Shah et al. reported mechanical properties of extruded composites using several kinds of fibers (Shao et al.1995, Shao & Shah 1997 and Akkaya et al. 2000). Figure 9 shows a comparison of the data of Shah et al. and our experimental results obtained in this study for extruded polypropylene (PP) and poly vinyl alcohol (PVA) discontinuous fiber composites. In literatures (Shao et al.1995, Shao & Shah 1997 and Akkaya et al. 2000), no detailed information of the fiber distribution has been reported. Then $V_{f,real}$ indicate in Figure 8 for the comparison purpose. Our data of PVA fiber composite is made of PVA fiber with $d_f = 0.040\text{mm}$, $L_f = 6\text{mm}$, $\sigma_f = 1600\text{MPa}$, and $E_f = 40\text{GPa}$. Except for the matrix and the composite of $V_{f,real} = 2\%$ tested in this study, all of the composites have shown pseudo strain-hardening.

It should be mentioned here that excessive addition of discontinuous fibers cause a decrease of ultimate tensile stress and strain, as illustrated in Figure 8 and 9. The largest volume fraction of $V_{f,real} = 8.4\%$ results in the ultimate tensile stress is slightly decreased. This observation may suggest that there is an optimal fiber volume fraction for the mechanical properties of extruded discontinuous fiber reinforced composites. As shown in Figure 9, our composites with higher tensile stress show a smaller strain capacity are compared with the composite prepared by Shah et al. In addition, the density of the

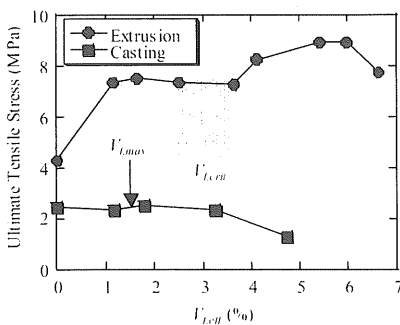


Figure 8. Dependence of ultimate tensile stress of the extruded and cast composites on $V_{f,eff}$.

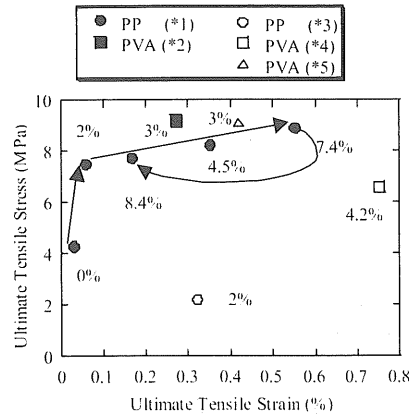


Figure 9. Comparison of the data in this paper and other researchers: *1: this paper, *2: Takashima et al. 2001, *3 Shao et al. 1995, *4: Shah and Shao 1997, *5 Akkaya et al. 2000.

composites is significantly smaller than that of Shah et al.

Wu & Li (1994) have shown that it becomes more difficult to induce multiple cracking in the case of high matrix toughness. This is the case for our fiber composites. Further improvement in the mechanical properties, particularly for enhancement strain capacity calls for tailoring the interfacial properties.

5 CONCLUSIONS

In this paper, we presented a basis of micromechanics model of the design for the mechanical properties of aligned fiber reinforced composite, especially the critical volume fraction for pseudo strain-hardening. In order to support the micromechanics model, uniaxial tension tests were conducted on polypropylene discontinuous fiber reinforced cementitious composites manufactured by extrusion molding. The critical volume fraction was determined experimentally from ultimate tensile strain and number of multiple cracks versus fiber volume fraction relationship. The theoretical volume fraction predicted by the micromechanics model for the extruded composite reasonably agreed with the experimental data.

For comparison, the cast fiber reinforced composites were tested in addition to the extruded composites. A comparison of the extruded and cast fiber composites indicated that the extrusion molding allows us to incorporate larger volume of fibers and to improve the mechanical properties of fiber composites compared to the conventional casting. The highest ultimate tensile stress of our extruded fiber composite reached 8.9MPa and the strain capacity was up to 0.55%.

REFERENCES

- Aveston, J & Kelly, A. 1973 Theory of multiple fracture of fibrous composites. *Journal of Material Science* Vol.8 352-362.
- Li, V.C. et al. 1991 A micromechanical model of Tension softening and bridging toughening of short random fiber reinforced brittle matrix composites. *J. Mech. Phys. Solids* Vol.39 (5): 607-625.
- Li, V.C. 1992a Postcrack sealing relations for fiber reinforced cementitious composites. *Journal of Materials in Civil Engineering* Vol.4 (1): 41-57.
- Li, V.C. & Leung, C.K.Y. 1992b. Steady-State and Multiple Cracking of random fiber composites. *Journal of Engineering Mechanics* . Vol.118 (11): 2246-2264.
- Stang, H. et al. Design and structural applications of stress-crack width relations in fibre reinforced concrete. *Materials and Structures* Vol.28 210-219.
- Kabele, P & Horii, H. 1996 Analytical model for fracture behaviors of pseudo strain-hardening cementitious composites. *J. Mat. Conc Struct. Pervements.*, JSCE. Vol.30 (532) 209-219.
- Li, V.C. & Hashida, T. 1993 Engineering ductile fracture in brittle-matrix composites. *Journal of Materials Science Letter* 12: 898-901.
- Kanda et al. 2000 Tensile stress-strain modeling of pseudo-strain hardening cementitious composites. *Journal of Materials in Civil Engineering* Vol.12 (2) 147-156.
- Stang, H. & Pedersen, C. HPRCC - Extruded Pipes *Materials for the New Millennium*. Vol.1 261-270.
- Mu, B. & Li, Z.J. 1998 Tensile failure of short fiber-reinforced composites. *Key Engineering Materials* Vol.145-149: 607-612.
- Li, Z. et al. 1999 Prediction of overall tension behavior of short fiber-reinforced composites. *International Journal of Solids and Structures* Vol. 36: 4071-4087.
- Shah, S.P. & Shao, Y. 1994 Extrusion processing of fiber-reinforced cement-matrix composites. *ASME MD* Vol.52: 205-216.
- Shao, Y et al. 1995 Extruded fiber-reinforced composites. *Concrete International* April: 48-52.
- Akkaya et al. 2000 Parameters related to fiber and processing in cementitious composites. *Materials and Structures* Vol.33: 515-524.
- Li, V. C. 1993 From micromechanics to structural engineering - The design of cementitious composites for civil engineering applications. *JSCE J. of Structural. Mech. Earthquake Eng.* Vol.10 (2): 37-48.
- Marshall, D. B. & Cox, B. N. 1988 A J-integral method for calculation steady-state matrix cracking stresses in composites. *Mechanics of Materials* Vol.7: 127-133.
- Li, V.C. & Chan, Y-W. 1994 Determination of interfacial debond mode for fiber-reinforced cementitious composites. *Journal of Engineering Mechanics* Vol.120 (4): 707-719.
- Kanda, T. & Li, V.C. 1998 Interface property and apparent strength of high-strength hydrophilic fiber in cement matrix. *Journal of Materials in Civil Engineering* Vol.10(1): 5-13.
- Milewski, J.V. 1974 A study of the packing of milled fiber-glass and glass beads. *Polymer-Plast. Technol. Eng.* Vol.3(1): 101-120.
- Evans, K.E. & Gibson, A.G. 1986 Prediction of the maximum packing fraction achievable in randomly oriented short-fibre composites. *Composites Science and Technology* Vol.25: 149-162.
- Shao, Y & Shah, S.P. 1997 Mechanical properties of PVA fiber reinforced cement composites fabricated by extrusion processing. *ACI Materials Journal* Vol.94(6): 555-564.

- Takashima et al. 2001 PVA fiber rupture in the extruded cementitious composites. (in preparation)
- Wu, H-C. & Li, V.C. 1994 Trade-off between strength and ductility of random discontinuous fiber reinforced cementitious composites. *Cement & Concrete Composites* Vol.16: 23-29.

APPENDIX

Single Fiber Stress - Displacement Curve for aligned fiber reinforced composite

Consider a single fiber with a diameter d_f , length L_f , an interfacial friction bond strength τ and the snubbing coefficient f . The elastic modulus of matrix and fiber are E_m, E_f , respectively and the volume fraction matrix and fiber are V_m, V_f , respectively.

Li et al. (1991) showed that the bridging stress-displacement curve can be predicted by integrating the contribution of individual fibers crossing a matrix crack plane:

$$\sigma_B(\delta) = \frac{4V_f}{\pi d_f^2} \int_{\varphi=0}^{\pi} \int_{z=0}^{L_f} P(\delta) p(\varphi) p(z) dz d\varphi \quad (13)$$

where $P(\delta)$ = the fiber bridging load versus displacement δ , $p(\varphi)$ and $p(z)$ = probability-density function of the orientation angle and centroidal distance of fibers from crack plane.

Li (1992a) has shown that during frictional debonding, the fiber-bridging load versus displacement can be obtained from a shear-lag analysis:

$$P(\delta) = \frac{\pi}{2} \sqrt{(1+\eta)E_f d_f^3 \tau \delta} e^{-\eta \delta} \text{ for } \delta \leq \delta_0 \quad (14)$$

where $\delta_0 \equiv (4l^2\tau) / [(1+\eta)E_f d_f]$ correspond to the displacement at which frictional debonding is completed for a fiber with embedment length l and $\eta \equiv (V_f E_f / V_m E_m)$.

After the fiber is fully debonded, a fiber pullout load versus displacement curve can be given by a following equation (Li 1992a):

$$P(\delta) = \pi \tau l d_f \left(1 - \frac{\delta}{l}\right) e^{-\eta \delta} \text{ for } \frac{l}{2} \geq \delta \geq \delta_0 \quad (15)$$

For uniformly aligned fiber distribution ($\varphi = 0$), $p(\varphi) = 1$ and $p(z) = 2/L_f$ (Li et al. 1991). Using eqs. (14) and (15) in eq. (13), the prepeak part of the bridging stress-displacement curve can be obtained in normalized form:

$$\tilde{\sigma}_B(\tilde{\delta}) = 2 \left[2 \left(\frac{\tilde{\delta}}{\tilde{\delta}^*} \right)^2 - \frac{\tilde{\delta}}{\tilde{\delta}^*} \right] \text{ for } \tilde{\delta} \leq \tilde{\delta}^* \quad (16)$$

where $\tilde{\sigma}_B \equiv \sigma_B/\sigma_0$, $\sigma_0 \equiv V_f \tau (L_f / d_f)/2$, and $\tilde{\delta} \equiv \delta / (L_f / 2)$. $\tilde{\delta}^*$ $\equiv [2\tau / (1+\eta) E_f](L_f / d_f)$ corresponds to the maximum attainable value of δ_0 normalized by $L_f / 2$ for the fiber with the longest embedment length of $L_f / 2$.

The postpeak part of the bridging stress–displacement curve can be obtained in normalized form:

$$\tilde{\sigma}_B(\tilde{\delta}) = 2(1 - \tilde{\delta})^2 \text{ for } 1 > \tilde{\delta} > \tilde{\delta}^* \quad (17)$$

The maximum value σ_{pc} of the bridging stress–displacement curve is $\frac{2}{3}\sigma_0$ that is obtained from eq. (14) by setting $\tilde{\delta}$ into $\tilde{\delta}^*$.

$$\sigma_{pc} = \tau V_f \left(\frac{L_f}{d_f} \right) \quad (18)$$

The fracture energy due to fiber bridging stress

The debonding part of the fracture energy can be estimated by the following equation with σ_B given by eq. (16).

$$G_r = \int_0^{\delta^*} \sigma_B(\delta) d\delta = \frac{5}{3} \sigma_0 \delta^* \quad (19)$$

The fracture energy due to fiber pullout can be given by the following equation with σ_B given by eq.(17).

$$G_c = \int_{\delta^*}^{L_f/2} \sigma_B(\delta) d\delta = 2\sigma_0 \left\{ \frac{1}{3} \left(\frac{L_f}{2} \right) - \delta^* \right\} \quad (20)$$

The fracture energy due to fiber bridging stress can be obtained from eqs. (19) and (20).

$$G_b = G_r + G_c = \frac{\sigma_0}{3} (L_f - \delta^*) \approx \frac{1}{6} \tau V_f d_f \left(\frac{L_f}{d_f} \right)^2 \quad (21)$$

where δ^* is neglected when $\delta^* \ll L_f$.